Modeling microlenses by use of vectorial field rays and diffraction integrals

Miguel A. Alvarez-Cabanillas, Fang Xu, and Yeshaiahu Fainman

A nonparaxial vector-field method is used to describe the behavior of low-*f*-number microlenses by use of ray propagation, Fresnel coefficients and the solution of Maxwell equations to determine the field propagating through the lens boundaries, followed by use of the Rayleigh–Sommerfeld method to find the diffracted field behind the lenses. This approach enables the phase, the amplitude, and the polarization of the diffracted fields to be determined. Numerical simulations for a convex–plano lens illustrate the effects of the radii of curvature, the lens apertures, the index of refraction, and the wavelength on the variations of the focal length, the focal plane field distribution, and the cross polarization of the field in the focal plane.

OCIS codes: 080.3630, 220.3630, 260.1960.

1. Introduction

Low-*f*-number ($f/\#$) microlenses have become increasingly important in optical and optoelectronic applications such as free-space optical interconnection, laser beam shaping, and fiber-optic communications. High system-packaging density requires low-$f/\#$ microlenses; for example, the efficient collimation of single-mode vertical-cavity surface-emitting lasers requires low-$f/\#$ (e.g., below $f/2$) microlenses. Furthermore, advanced microfabrication technologies[1,2] increasingly rely on our ability to accurately model and design low-$f/\#$ microlenses.

Current lens analysis tools use geometrical optics, scalar diffraction theory, and rigorous vector-field diffraction theory. Although geometrical optics is very successful in modeling large lenses, scalar diffraction theory (Kirchhoff integral approach) is used to investigate the far-field wave propagation phenomena. It is common in geometrical and scalar wave optics to characterize a lens by its $f/\#$, defined as the ratio of the focal length (f) and the diameter (D) of the lens.

In addition, scalar diffraction theory introduces a Fresnel number $N = D^2/4\lambda f$, where λ is the wavelength of the optical field. As the aperture of the lens decreases, the actual focal length of the lens shifts (toward the lens) from its geometric focal length. This effect, initially associated with a small $f/\#$,[3] was later attributed to the small Fresnel number as shown by Li and Wolf,[4] who solved the scalar diffraction of spherical waves by an aperture with a small Fresnel number (i.e., $N < 10$). The Rayleigh–Sommerfeld approach[5,6] was used to improve the accuracy of the scalar diffraction from lenses with $f/\# > 1$. Additionally, Hsu and Barakat[7] applied vector-field diffraction theory to solve diffraction by apertures with small Fresnel numbers within the Fresnel region. This approach considers only the fields at the aperture that converge to a focus. Wang and Prata[8] started from the same approach and built a coupled-field integral equation that relies on a computationally intensive method of moments. In this paper we model low-$f/\#$ microlenses as well as lenses with small Fresnel numbers.

Early work in vectorial treatments of diffraction of a convergent spherical wave at a circular aperture was conducted by Richards and Wolf.[9] Recently, Gu[10] and Chon *et al.*[11] applied an extension of the Debye theory to a high numerical aperture, finding important contributions made by the longitudinal component of the field in the focal region. Lax[12] showed that the longitudinal component of the field in the propagation direction is a requirement for the solution of the Maxwell equations for paraxial beam propagation; the nonparaxial beam was shown by Cao *et al.*[13,14] The measurement of the longitudinal

M. A. Alvarez-Cabanillas (m.alvarez@osa.org) is with the Instituto Politécnico Nacional, Digital Technology Research and Development Center, Avenida del parque 1310, Tijuana B.C. México, 22510. F. Xu and Y. Fainman are with the Department of Electrical and Computer Engineering, University of California, San Diego, California 92093.

Received 20 August 2003; revised manuscript received 12 January 2004; accepted 15 January 2004.

0003-6935/04/112242-09$15.00/0

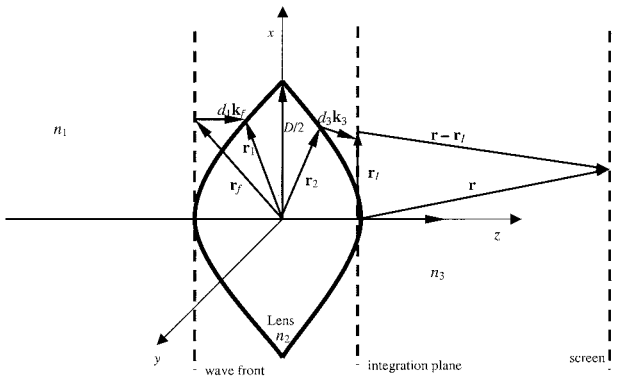

Fig. 1. Incident beam in a homogeneous medium with a refractive index of n_1 is introduced into a lens of diameter D made from material with a refractive index of n_2 and radii of curvature R_1 and R_2. The diffracted beam propagates in the homogeneous medium with a refractive index of n_3.

component of the diffracted fields by lenses in the microwave region was made by Carswell.[15]

In this paper we develop a vector-field modeling method that allows the investigation of the transmission of polarized light. In comparison with existing vector-field modeling tools, our method is less computationally intensive than other numerical methods [finite-element method (FEM), method of moments (MOM), finite-difference time domain (FDTD), etc.] for general applications. These numerical methods require that one finds the field at each node of a mesh that is distributed through the three-dimensional space. In contrast, our method depends only on the number of rays (i.e., that the number of nodes $\gg$ number of rays) and therefore can easily be utilized in microlens modeling.

A detailed comparison of our method with other existing numerical methods is beyond the scope of this work. However, as an example, we calculated the diffracted field of a microlens by using our proposed technique and compared it with that obtained with the FDTD method in the same computational environment. We found that our method was approximately 245 times faster than that obtained with the two-dimensional FDTD method. Compared with scalar theory, our method can be more accurate, as indicated in Section 4. Furthermore, our proposed method produced the same results as those obtained by the vectorial diffraction applied by Hsu and Barakat.[7] Our technique is based on the transformation of the fields between the dielectric boundaries of the lens surfaces by satisfying the boundary conditions, followed by the calculation of the vector field of the diffracted fields by using the Rayleigh–Sommerfeld theory.

Our method considers the effects of the radius of curvature and aperture of the lens, the index of refraction of the media, and incident optical field characteristics such as phase, amplitude, polarization, and wavelength (see Fig. 1). Although the formulations of this method are derived for an arbitrary incident field distribution (i.e., spatial distribution and propagation directions), the numerical examples focus on the refraction of a polarized plane wave by a convex–plano microlens. This type of microlens is commonly used in practical applications. To calculate the modification of the incident fields by the microlens, we obtain the wave propagation of the field through the lens by ray tracing, in which each ray tracing is associated with a solution of the Helmholtz equation.

The wave vector, initially defined by the incident wave front, determines the propagation of the ray. The medium on each side of the boundary is considered to be isotropic and homogeneous; consequently, the wave vector is not modified within each medium. The transmitted and reflected fields and their associated wave vectors at each boundary are calculated. The fields diffracted by the lenses are calculated by use of Rayleigh–Sommerfeld theory such that the finite aperture of the lens and the vectorial behavior of the field are considered. We define an integration plane at the exit pupil of the lens. We assume that the electromagnetic field vanishes outside the illuminated area in this integration plane and that the fields within this area must satisfy the Neumann or Dirichlet boundary condition so that the equations that describe the diffracted wave are mathematically consistent.[16]

In Section 2 we derive expressions for calculating the cross-boundary field within the media. The method treats each point as a solution of the Helmholtz equation and provides by means of local ray tracing, the transmitted and the reflected fields and their associated wave vectors at each boundary. In Section 3, we obtain the expression for the Rayleigh–Sommerfeld integral in its exact form as well as under the Fresnel and Fraunhofer approximations. The approximations were made with respect to the distance between the aperture and each diffracted field at the screen.

An alternative method for calculating the diffracted fields by circular apertures was proposed by Harvey,[17] Southwell,[18] and Sheppard and Hrynevych.[19] Section 4 presents the numerical simulation results of the diffracted field and its dependence on the lens aperture and radius of curvature, the wavelength of the incident light, and the polarization of light. A summary and conclusions are provided in Section 5.

2. Field Ray Propagation Formulation

Consider a circular lens of diameter D with a pupil shape defined by the spatial function $\mathbf{r}_1(r)$ for the entrance pupil and $\mathbf{r}_2(r)$ for the exit pupil, respectively. The lenses studied here are on-axis lenses, and the origin of the coordinate system is chosen at the lens axes. The monochromatic plane wave that reaches the lens has a wave vector $\mathbf{k}_f(\mathbf{r}_f) = k_f\mathbf{x}_3$ and is linearly polarized.

The space is divided in three regions with refractive indices n_1, n_2, and n_3 (see Fig. 1). Region 1 contains the incident and the reflected fields; region 2 contains the fields inside the lens media; and region

3 contains the diffracted fields. R_1 is the radius of curvature of the interface between regions 1 and 2, and R_2 is the radius of curvature of the interface between regions 2 and 3 (see Fig. 1). The electric field E at each point of the space is obtained from the solution of the Helmholtz equation given by

$$\nabla^2 E_i + k_i^2 E_i = 0, \qquad i = 1, 2, \text{ or } 3. \tag{1}$$

We assume that each medium is isotropic and homogeneous, allowing us to use ray tracing techniques to transfer the field distribution across the boundaries. The ray is associated with a local plane wave. A plane wave that satisfies Eq. (1) can be written as

$$\mathbf{E}_1(\mathbf{r}_f) = E_0 \exp(-j\mathbf{k}_1 \cdot \mathbf{r}_f)\mathbf{x}_2, \tag{2}$$

where $\mathbf{x}_2$ is the incident unit vector that it is defined by the polarization of the incident field and $\mathbf{r}_f$ defines the spatial distribution of the wave front when the incoming pupil is intersected at one point for the wave front (see Fig. 1). To facilitate the transformation of the incident fields through the lens boundaries, we define an orthogonal basis for the decomposition of the electromagnetic field in s and p polarization in the plane of incidence. This basis is defined in the plane of incidence by use of the incident-field unit wave vector $\mathbf{e}_{1f} = \mathbf{x}_3$ and the normal-to-the-entrance-pupil vector $\mathbf{e}_1$, defined in Eq. (A4) in Appendix A. The basis for the field at the entrance of the pupil is defined by the unit vectors, which are given by

$$\mathbf{e}_{1s} = -\frac{y_1}{\rho_1}\mathbf{x}_1 + \frac{x_1}{\rho_1}\mathbf{x}_2, \tag{3}$$

$$\mathbf{e}_{1p} = -\frac{x_1}{\rho_1}\mathbf{x}_1 - \frac{y_1}{\rho_1}\mathbf{x}_2, \tag{4}$$

$$\mathbf{e}_{1t} = \frac{(R_1^2 - \rho_1^2)^{1/2}}{R_1\rho_1}(x_1\mathbf{x}_1 + y_1\mathbf{x}_2) + \frac{\rho_1}{R_1}\mathbf{x}_3, \tag{5}$$

where $\rho_1 = \sqrt{x_1^2 + y_1^2}$ is over the entrance pupil, the unit vector $\mathbf{e}_{1s}$ is for the s polarization obtained from the vector product of $\mathbf{e}_1$ and $\mathbf{e}_1$; the unit vector $\mathbf{e}_{1p}$ for p polarization is obtained from the vector product of $\mathbf{e}_{1f}$ and $\mathbf{e}_{1s}$; and $\mathbf{e}_{1t}$ is a unit tangent to the first interface and is obtained from the vector product of $\mathbf{e}_{1s}$, $\mathbf{e}_{kf}$, and $\mathbf{e}_1$ (see Fig. 2).

In general the incident field at the first pupil can be described by

$$\mathbf{E}_1(\mathbf{r}_1) = E_{1s}(\mathbf{r}_1)\mathbf{e}_{1s} - E_{1p}(\mathbf{r}_1)\cos\alpha_1\mathbf{e}_{1t} + E_{1p}(\mathbf{r}_1)\sin\alpha_1\mathbf{e}_1, \tag{6}$$

where the field components are defined by

$$E_{1s}(\mathbf{r}_1) = E_0 \exp(-jk_1d_1)\frac{x_1}{\rho_1},$$

$$E_{1p}(\mathbf{r}_1) = -E_0 \exp(-jk_1d_1)\frac{y_1}{\rho_1}, \tag{7}$$

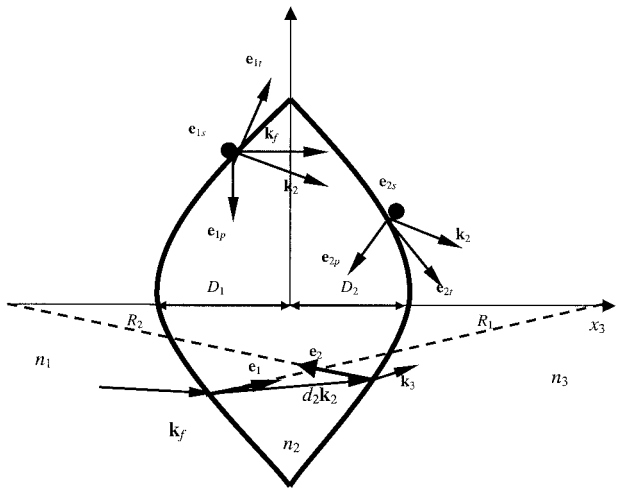

Fig. 2. Representation of unit vectors on the lens boundaries.

where α_1 is the angle between the incident ray and the normal vector $\mathbf{e}_1$ [see Eq. (A5)]. d_1 is the spatial shift between the wave front of the incident beam and the entrance pupil and is obtained from

$$d_1 = R_1 - \sqrt{R_1^2 - \rho_1^2}. \tag{8}$$

The transmitted wave vectors are defined by

$$k_2\mathbf{e}_{2k} = k_2 \sin\Omega_1\mathbf{e}_{1t} + k_2 \cos\Omega_1\mathbf{e}_1, \tag{9}$$

where Ω_1 is the refracted angle defined in Eq. (A5) in Appendix A and $k_2 = 2\pi n_2/\lambda$. The incident fields at the second interface are given by

$$\mathbf{E}_2(\mathbf{r}_2) = T_{1s}E_{2s}(\mathbf{r}_2)\mathbf{e}_{1s} - T_{1p}E_{2p}(\mathbf{r}_2)\cos\Omega_1\mathbf{e}_{1t} + T_{1p}E_{2p}(\mathbf{r}_2)\sin\Omega_1\mathbf{e}_1, \tag{10}$$

where

$$E_{2m}(\mathbf{r}_1) = \exp(-jk_2d_2)\mathbf{E}_1 \cdot \mathbf{e}_{1m}, \tag{11}$$

where $m = s$ or p. T_{1s} and T_{1p} are the transmission coefficients for s and p polarization, which are defined in Eq. (A6) in Appendix A. d_2 is the path length of the ray from the entrance pupil to the exit pupil (see Fig. 2) and is obtained from

$$d_2 = \frac{D_1 - R_1 + \sqrt{R_1^2 - \rho_1^2}}{\cos\alpha_2}, \tag{12}$$

where $\alpha_2 = \alpha_1 - \Omega_1$ is the angle between the incident and the refracted ray. The thicknesses D_1 and D_2 for the entrance and exit pupils, respectively, are defined by

$$D_1 = R_1 - \left(R_1^2 - \frac{D^2}{4}\right)^{1/2},$$

$$D_2 = R_2 - \left(R_2^2 - \frac{D^2}{4}\right)^{1/2}. \tag{13}$$

The fields that are transmitted through the second interface are obtained by the following procedure,

which is similar to the calculation of the resultant fields in the interaction with the first interface. We define a plane of integration at the exit pupil in region 3. This plane is transversal to its optical axis and tangent to the exit pupil. The transmitted fields at the integration plane are given by

$$\mathbf{E}_3(\mathbf{r}_2) = T_{2s}E_{3s}(\mathbf{r}_2)\mathbf{e}_{2s} - T_{2p}E_{3p}(\mathbf{r}_2)\cos\,\Omega_2\mathbf{e}_{2t} + T_{2p}E_{3p}(\mathbf{r}_2)\sin\,\Omega_2\mathbf{e}_2, \tag{14}$$

where

$$E_{3m}(\mathbf{r}_2) = \mathbf{E}_2 \cdot \mathbf{e}_{2m}\exp(-jk_3d_3), \tag{15}$$

where $m = s$ or p. $\mathbf{E}_3$ is the transmitted field from the second interface of the microlens, and the distance d_3 from the exit pupil to the plane (see Fig. 1) is obtained from

$$d_3 = (D_2 - \mathbf{r}_2 \cdot \mathbf{x}_3)/\mathbf{e}_{3k} \cdot \mathbf{x}_3. \tag{16}$$

For a convex–plano lens a special case was used in our numerical results (see Section 4). The unit vectors at the exit pupil are defined by

$$\mathbf{e}_{2s} = \mathbf{e}_{1s}, \qquad \mathbf{e}_{2t} = -\frac{x_1}{\rho_1}\mathbf{x}_1 - \frac{y_1}{\rho_1}\mathbf{x}_2,$$
$$\mathbf{e}_2 = -\mathbf{x}_3, \qquad d_3 = 0. \tag{17}$$

In this section we obtained the field over the exit pupil by considering three media with different indices of refraction, the geometrical shape of the interfaces, and their effects on the phase and polarization of the incident beam. In Section 3 we consider the effect of diffraction.

3. Rayleigh–Sommerfeld Diffraction

The field diffracted by the microlens is obtained by the application of the Rayleigh–Sommerfeld integral over each component of the field in the integration plane

$$\mathbf{E}_I(\mathbf{r}_I) = E_1(x_I, y_I, z_I)\mathbf{x}_1 + E_2(x_I, y_I, z_I)\mathbf{x}_2 + E_3(x_I, y_I, z_I)\mathbf{x}_3,$$

obtained from Eq. (15). The integration area S_I is bounded by a finite aperture because the fields vanish outside this illuminated aperture.

Consequently, we may apply the Dirichlet boundary conditions to the Rayleigh–Sommerfeld integral to obtain the diffracted fields

$$\mathbf{E}(\mathbf{r}) = \int_{S_I} \mathrm{d}s\mathbf{E}(\mathbf{r}_I)\frac{\partial}{\partial n}G(\mathbf{r}_I, \mathbf{r}), \tag{18}$$

where $\mathbf{E}(\mathbf{r}_I)$ is the field distribution in the integration plane defined by Eq. (14), $\partial/\partial n$ is the transversal derivative to the integration plane, and $G(\mathbf{r}_I, \mathbf{r})$ is the Green function for a spherical wave in free space:

$$G(\mathbf{r}_I, \mathbf{r}) = -\exp[-j(\mathbf{r} - \mathbf{r}_I)\mathbf{k}_3]/(2\pi|\mathbf{r} - \mathbf{r}_I|). \tag{19}$$

Equation (18) with the derivative applied to Eq. (19) can be rewritten as

$$\mathbf{E}(\mathbf{r}) = -\int_{S_I} \mathrm{d}s[\mathbf{E}(\mathbf{r}_I)/(2\pi|\mathbf{r} - \mathbf{r}_I|^2)][jk_3 + 1/|\mathbf{r} - \mathbf{r}_I|] \times [(\mathbf{r} - \mathbf{r}_I)\mathbf{e}_I]\exp[-j\mathbf{k}_3(\mathbf{r} - \mathbf{r}_I)], \tag{20}$$

where each component of the diffracted fields must satisfy the Sommerfeld radiation condition. The goal here is to obtain the diffracted fields in the focal region; thus, for a microlens, $|\mathbf{r}|$ is of the order of tens of wavelengths, where the integral at Eq. (20) shows good behavior. To make the numerical integration, a mesh is defined over the integration plane with cells of area Δs. The vector field rays arriving at the cell are added and associated to this area. Thus Eq. (20) is solved by applying a standard surface numerical integration.

In the practical situations, $r = |\mathbf{r}|$ is large compared with the illuminated aperture in the integration plane ($|\mathbf{r}| > |\mathbf{r}_I|$), making Fresnel and Fraunhofer approximations valid for simplifying the expressions for the diffracted fields. The approximations are made with respect to the distance between the aperture and each diffracted field at the screen. In the Fresnel approximation we keep the quadratic terms for the exponent, but drop the terms of higher degree [see Appendix A, Eq. (A9)]. In the denominator of Eq. (20) we drop the quadratic and higher-order terms. The diffracted fields in the Fresnel approximation are given by

$$\mathbf{E}(\mathbf{r}) = -j[k_3(z - z_1)/(2\pi r^2)]\exp[-jk_3r] \times \int_{S_I} \mathrm{d}s\mathbf{E}(\mathbf{r}_I)\exp[jk_3(\mathbf{r} \cdot \mathbf{r}_I - r_I^2/2)/r]. \tag{21}$$

Using the Fraunhofer approximation, we can simplify the Rayleigh–Sommerfeld equation by keeping only the linear terms for the exponent [see Appendix A, Eq. (A10)], but this approximation is valid only when $r \gg \rho_I$ (i.e., it is not valid at the focal region):

$$\mathbf{E}(\mathbf{r}) = -j[k_3(z - z_1)/(2\pi r^2)]\exp[-jk_3r] \times \int_{S_I} \mathrm{d}s\mathbf{E}(\mathbf{r}_I)\exp[jk_3(\mathbf{r} \cdot \mathbf{r}_I)/r]. \tag{22}$$

In this section we thus obtained the diffracted field and Fresnel and Fraunhofer approximations to simplify the expression.

4. Numerical Simulation Results

The behavior of a simple convex-plano lens is investigated by use of the modeling method introduced in Sections 2 and 3. We investigate the position and the field distribution in the focal plane of these lenses by considering their aperture and radius of curvature. In addition, the polarization behavior of these lenses is examined. In the text that follows, all units

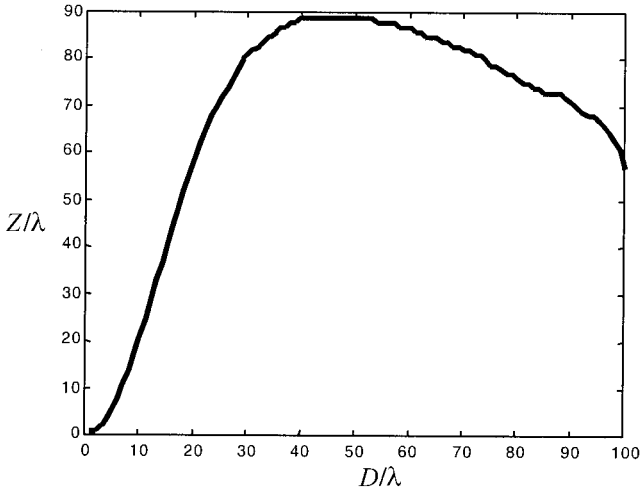

Fig. 3. Focal plane position as a function of the lens aperture for a lens with $R_1/\lambda = 50$, $R_2/\lambda = \infty$, and $n_2 = 1.5$.

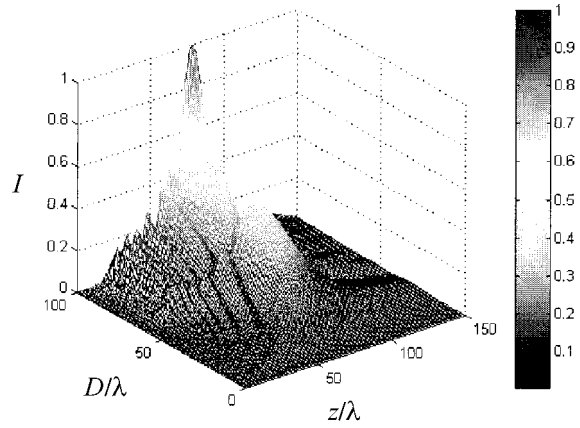

Fig. 4. Three-dimensional plot showing the lens aperture effect on the intensity distribution along the optical axis of a convex–plano lens. $R_1/\lambda = -50$, $R_2/\lambda = \infty$, $n_2 = 1.5$.

are normalized to the wavelength of the incident light unless otherwise stated.

A. Lens Aperture Effects

The aperture, the radii of curvature, and the refractive index of the lens determine the $f/\#$ and the Fresnel number of the lens. Conventionally, lenses with the same $f/\#$ perform identically in terms of depth of focus and focal spot size. However, as the aperture of the lens approaches the order of the wavelength, the behavior of the lens differs from that normally expected. The Fresnel number may be applied at this point to quantify the limit. Figure 3 illustrates the effect of lens aperture on the position of the focal plane of a lens with a fixed radius. The Brewster angle is obtained at the incident pupil when

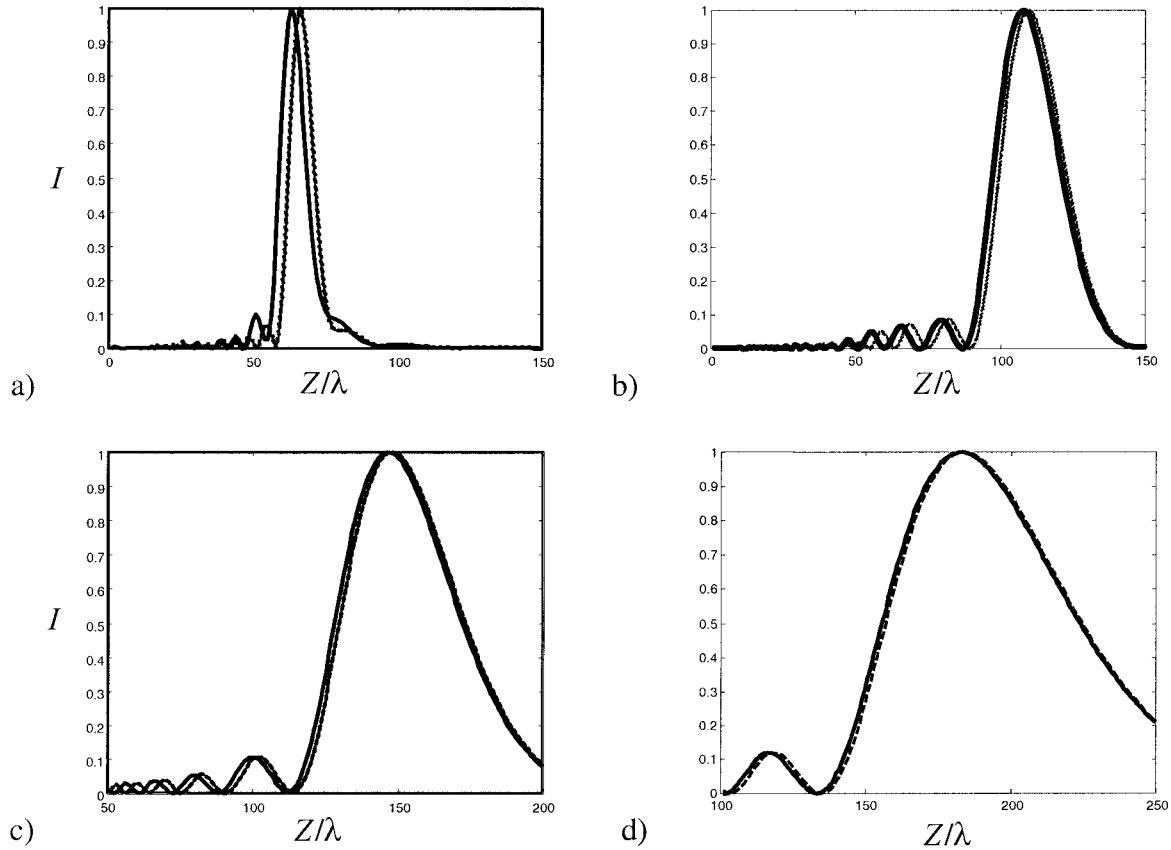

Fig. 5. Performance of the lens changes as the radius of curvature varies for the rigorous solution (solid curve) and for the Fresnel approach (dashed curve). ($D/\lambda = 60$ for all cases). (a) $R/\lambda = 40$, (b) $R/\lambda = 60$, (c) $R/\lambda = 80$, (d) $R/\lambda = 100$.

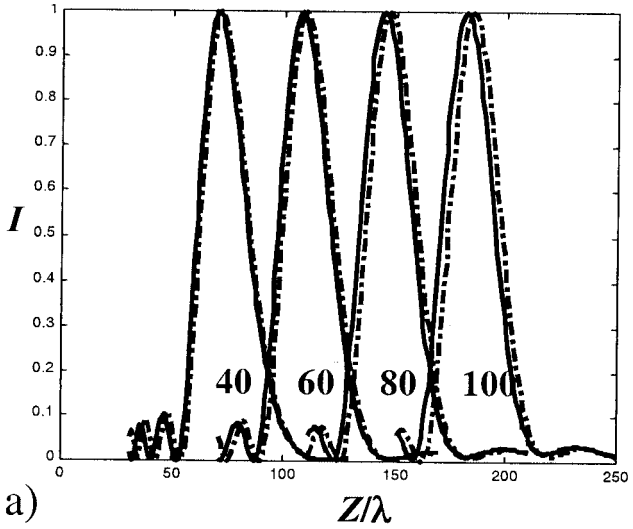

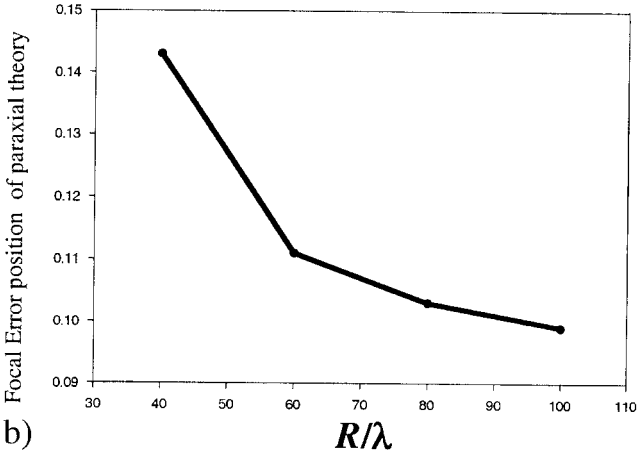

Fig. 6. Four lenses with the same $f/\#$, but different radii of curvature R/λ (40, 60, 80, and 100), have slightly different performances. (a) Intensity without the paraxial approximation (solid curves) and the Fresnel approximation (dashed curves). (b) Error of the focal position of the paraxial approximation.

$D = 83.2\ \lambda$, and the critical angle for the exit pupil is obtained when $D = 99.3\lambda$, as is shown in Fig. 3. The paraxial approximation predicts a focal length of 100 for this radius of curvature. The numerical simulation results indicate that when the aperture of the lens is approximately 40–50, the focal length is approximated by the paraxial approximation. However, when the aperture becomes large, paraxial approximation fails. That spherical aberration dominates is clear from the results shown in Fig. 4.

When the aperture is smaller than 40, the Fresnel number becomes small (less than 4), spherical aberration dominates, and the diffraction effects are stronger than the focusing power of the lens. The end result is that the focusing effect does not take place. This result is further illustrated in Fig. 4(a), which shows that, in general, the larger the aperture, the more intense the focal point. However, due to lower reflection around Brewster angle, there is a region for which this trend is violated.

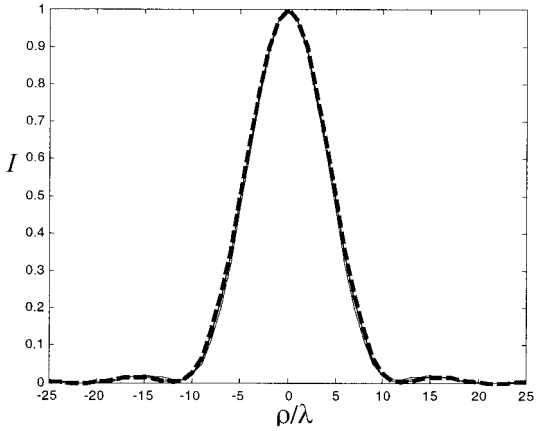

Fig. 7. Lenses with the same $f/\#$ produce the same spot size at their focal planes.

It is well known that the focal length of a convex–plano lens varies as its radius of curvature changes. The focal length of the lens under the paraxial approximation is determined by the curvature and the refractive indices of the materials of the lens and the surrounding medium. Our simulation results shown in Figs. 4 and 5 indicate that the position of the focal plane of a lens is determined not only by the radius of curvature and the refractive index of the lens, but also by the aperture effects of the lens. This makes the $f/\#$ parameter difficult to calculate because the exact focal length cannot be easily predicted. Therefore, for microlenses, the definition of the $f/\#$ by use of the focal length obtained from the paraxial approximation needs to be carefully examined.

B. Radius of Curvature Effects

Lenses with the same aperture but a different radius of curvature focus the light at different locations (see Fig. 5). It can easily be predicted that, compared with lenses with lower $f/\#$s [see Fig. 6], lenses with higher $f/\#$s may be more accurately modeled with the Fresnel approximation. However, results also show that lenses with the same ratio between the radius of curvature and the lens diameter (i.e., same $f/\#$ in the paraxial approximation) perform differently.

We modeled four convex–plano lenses with the same $f/\#$ (i.e., $f/2$) but with different curvatures, which are shown in Fig. 6. The errors introduced by the paraxial approximation's prediction of the focal-plane positions of these lenses with the same $f/\#$ are shown in Fig. 6(a).

The paraxial approximation produces more errors when the curvature is larger (when R is small). The Fresnel approximation also deviates more from the rigorous calculation when R/λ yields smaller values. The paraxial approximation is more accurate when R/λ is large. However, according to our investigation (see Fig. 7), these same $f/\#$ lenses produce the same focal spot size.

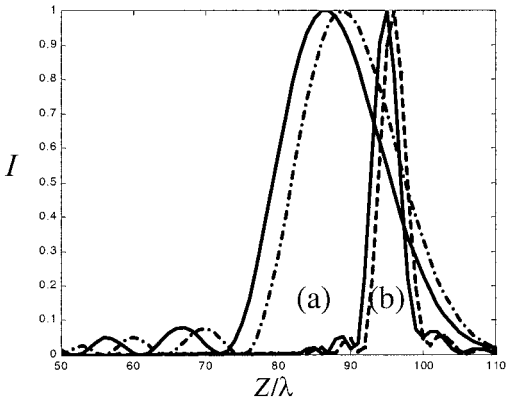

Fig. 8. Difference between the rigorous approach (solid curve) and the Fresnel approach (dashed curve) is greatly reduced when the wavelength is short. (a) $R = 50$ μm, D = 60 μm, λ = 1 μm; (b) $R = 50$ μm, D = 60 μm, λ = 0.1 μm.

C. Wavelength Effects

In geometrical optics the focal length of a lens does not depend on the wavelength of the incident light. Our studies reveal that the focal length of a microlens is a function of the wavelength. Figure 8 illustrates two extreme cases in which two wavelengths of ratio $\lambda_1/\lambda_2 = 10{:}1$ are incident on the same lens ($D/\lambda_1 = 60$ and $R/\lambda_1 = 50$). Note that the focal plane position is quite different in each case.

Shorter wavelengths focus closer to the position predicted by the paraxial approximation; however, the location is still quite different (i.e., f/λ_1 is 91 instead of 100). In addition, in analyzing the short-wavelength situation, the Fresnel approximation, which calculates an optical path length that is very close to the actual value, is accurate.

D. Polarization Effects

The ratio of the cross-polarization maximum is defined by

$$I_{xy} = 20 \log \frac{E_x}{E_y}, \qquad I_{zy} = 20 \log \frac{E_z}{E_y} \tag{23}$$

for an incident plane wave with polarization in the direction of the y-axis. The behavior of the cross polarization as a function of the curvature (R_1) with $D = 20\ \lambda$ and $n_2 = 3.5$ and of aperture (D) with $n_2 = 3.5$ and $R_1 = 50\ \lambda$ are shown in Figs. 9(a) and 9(b), respectively. Figure 9(c) shows the dependence of cross polarization on the microlens index (n_2) with $D = 20\ \lambda$ and $R_1 = 50\ \lambda$.

It is known that a curved surface may introduce polarization aberrations.[20] Our studies show that, when the plane wave is normally incident on a convex–plano lens, light polarization behavior depends on the input surface curvature. If the input field is a plane wave, then this approach predicts transversal cross polarization and longitudinal cross polarization according to the results of Lax,[12] Cao *et al.*,[13,14] and Carswell.[15] The longitudinal cross polarization is bigger than the transversal cross polarization in all of the cases shown in Fig. 9. Figure 9 also shows that the cross polarization decreases when the radius of curvature increases [Fig. 9(a)] and that the cross polarization increases when the aperture increases [Fig. 9(b)] or the index of the microlens increases [Fig. 9(c)].

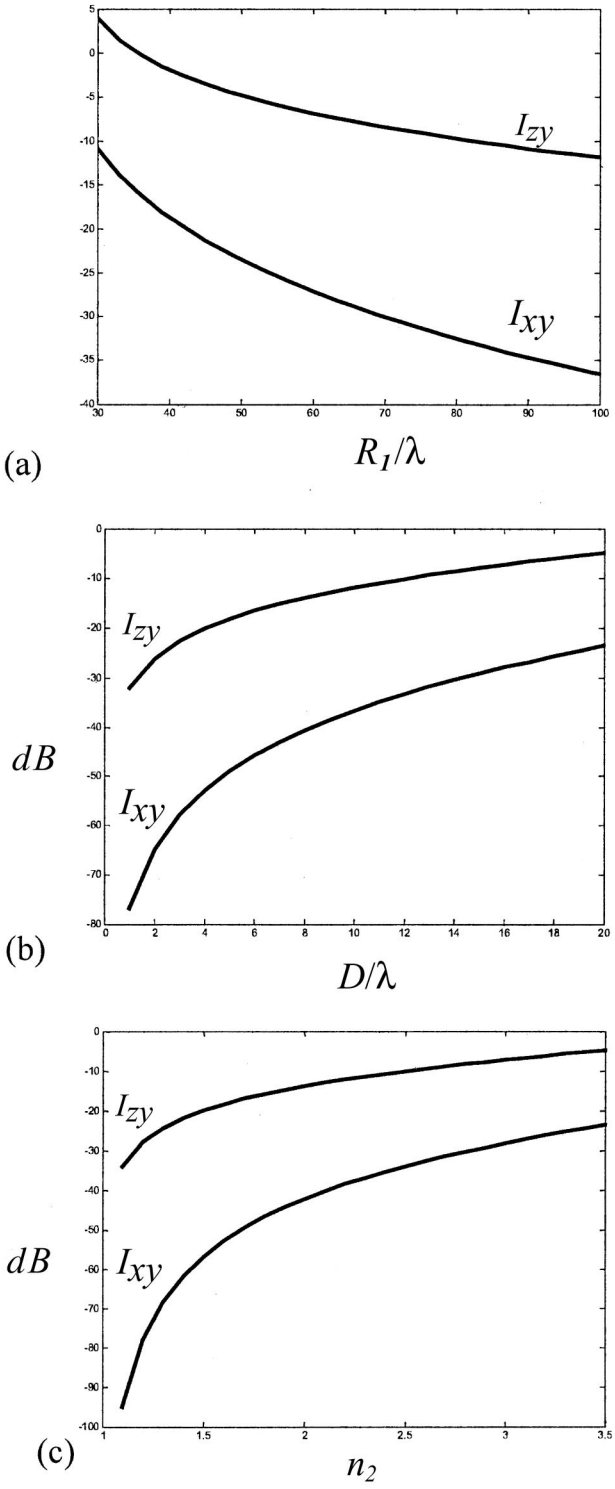

Fig. 9. Maximum cross polarization for (a) the variation of the curvature, (b) the variation of the aperture, and (c) the variation of the lens index.

5. Summary and Conclusions

A hybrid numerical modeling tool based on ray propagation of a vector field and on the Rayleigh–Sommerfeld diffraction theory was implemented to characterize the performance of low-f/# lenses, especially low-f/# microlenses. Simulation results indicate that the paraxial approximation is not valid, and rigorous modeling tools are essential to accurately model low-f/# microlenses. The effects of lens aperture, or Fresnel number, can be quite important for the design of microlenses. When the Fresnel number is below[7] 10 [or 4 for lenses made of glass (n = 1.5)] and the radius is 50λ, diffraction effect will override the focusing effect of the lenses. The focal length is a function of the radius of curvature, lens aperture, indices of refraction, wavelength, incident front wave, and polarization of the incident beam. The exact focal length is difficult to calculate because no analytical formula is available. Therefore, only the f/# in the paraxial theory may be used to estimate the performance of the lens. Moreover, lenses with the same radius of curvature to aperture ratio produce the spot size at the focal planes. This technique was used to obtain the transverse cross polarization and the longitudinal cross polarization according to the solution of the Maxwell equations for finite beams.[12] Furthermore, it was shown that convex–plano lenses produce polarization aberrations when a plane wave is normally incident on the curved surface. The technique presented here is general and can be applied to lenses with more complex and irregular pupil geometries, and the number of lenses in the system can be increased with a very small accompanying increase in processing time. The uniqueness of this technique is that it associates a field at each ray, its solution of the Maxwell equations satisfies the boundary conditions at each pupil, and it considers diffraction by use of the rigorous Rayleigh–Sommerfeld method, which, unlike the Kirchoff method, has a mathematical structure that facilitates its implementation in numerical algorithms. These characteristics give this technique the advantages of increased accuracy and decreased processing time, making it preferable to other techniques.

Appendix A

The entrance pupil is defined by $\mathbf{r}_1 = x_1\mathbf{x}_1 + y_1\mathbf{x}_2 + z_1\mathbf{x}_3$, where

$$z_1 = (R_1^2 - D^2/4)^{1/2} - (R_1^2 - x_1^2 - y_1^2)^{1/2} \quad \text{(A1)}$$

and $\mathbf{x}_1$, $\mathbf{x}_2$, and $\mathbf{x}_3$ are unit vectors. The unit normal vector to the surface of the entrance pupil is

$$\mathbf{e}_1 = -[x_1\mathbf{x}_1 + y_1\mathbf{x}_2 - (R_1^2 - x_1^2 - y_1^2)^{1/2}\mathbf{x}_3]/R_1. \quad \text{(A2)}$$

The exit pupil is defined by $\mathbf{r}_2 = x_2\mathbf{x}_1 + y_2\mathbf{x}_2 + z_2\mathbf{x}_3$, where

$$z_2 = (R_2^2 - x_2^2 - y_2^2)^{1/2} - (R_2^2 - D^2/4)^{1/2} \quad \text{(A3)}$$

and the unit normal vector to the surface of the exit pupil is

$$\mathbf{e}_2 = -[x_2\mathbf{x}_1 + y_2\mathbf{x}_2 + (R_2^2 - x_2^2 - y_2^2)^{1/2}\mathbf{x}_3]/R_2. \quad \text{(A4)}$$

The incident angle $\alpha_i(\mathbf{r}_i)$ at the i interface (entrance pupil) is defined from the incident wave vector $\mathbf{k}_i$ and the surfaces vector $\mathbf{e}_i$. Thus the refracted angle $\Omega_i(\mathbf{r}_i)$ is obtained from Snell's law and can be written by

$$\alpha_i(\mathbf{r}_i) = \cos^{-1}\mathbf{k}_i \cdot \mathbf{e}_i,$$
$$\Omega_i(\mathbf{r}_i) = \sin^{-1}(n_i \sin\alpha_i)/n_{i+1}, \quad \text{(A5)}$$

where $i = 1, 2$ defines the microlens interface (surface of the pupils).

The transmission coefficients for s and p polarization are given by

$$T_{is} = \frac{2n_i\cos\alpha_i}{n_i\cos\alpha_i + n_{i+1}\cos\Omega_i},$$
$$T_{ip} = \frac{2n_i\cos\alpha_i}{n_{i+1}\cos\alpha_i + n_i\cos\Omega_i}. \quad \text{(A6)}$$

The coordinate system is moved to the integration plane through the microlens axis. Under this coordinate system, the points where we want obtain the diffracted fields are given by

$$r^2 = \rho^2 + (z - z_I)^2, \qquad \rho^2 = x^2 + y^2, \quad \text{(A7)}$$
$$r_I^2 = x_I^2 + y_I^2$$

and

$$|\mathbf{r} - \mathbf{r}_1| = r[1 + (\mathbf{r}_I^2 - 2\mathbf{r} \cdot \mathbf{r}_I)/r^2]^{1/2}. \quad \text{(A8)}$$

To apply the Fresnel approximation, Eq. (A8) is expanded, keeping only the quadratic terms and resulting in (see Fig. 1)

$$\frac{1}{|r - r_I|} \approx \frac{1}{r},$$
$$\exp(-jk|\mathbf{r} - \mathbf{r}_I|) \approx \exp[-jk(r - \mathbf{r} \cdot \mathbf{r}_I/r + r_I^2/2r)], \quad \text{when } r > r_I. \quad \text{(A9)}$$

For the Fraunhoffer approximation, the linear term of Eq. (A9) is kept as

$$\frac{1}{|r - r_I|} \approx \frac{1}{r},$$
$$\exp(-jk|\mathbf{r} - \mathbf{r}_I|) \approx \exp[-jk(r - \mathbf{r} \cdot \mathbf{r}_I/r)], \quad \text{when } r \gg r_I. \quad \text{(A10)}$$

This study was supported in part by the National Science Foundation, the Defense Advanced Research Projects Agency, Applied Micro Circuits Corporation/California Communications Research Program, and the U.S. Air Force Office of Scientific Research.

References

1. E. Park, M. Kim, and Y. Kwon, "Microlens for efficient coupling between LED and optical fiber," IEEE Photon. Technol. Lett. **11,** 439–441 (1999).
2. S. Calixto and M. Ornelas-Rodriguez, "Mid-infrared microlenses fabricated by melting method," IEEE Photon. Technol. Lett. **17,** 1212–1214 (1999).
3. A. Walther, *The Ray and Wave Theory of Lenses* (Cambridge University, Cambridge, England, 1995).
4. Y. Li and E. Wolf, "Focal shift in diffracted converging spherical waves," Opt. Commun. **39,** 211–215 (1981).
5. M. A. Alonso, A. A. Asatryan, and G. W. Forbes, "Beyond the Fresnel approximation for focused waves," J. Opt. Soc. Am. A **16,** 1958–1969 (1999).
6. A. Wünsche, "Transition from the paraxial approximation to exact solution of the wave equation and application to Gaussian beams," J. Opt. Soc. Am. A **9,** 765–774 (1992).
7. W. Hsu and R. Barakat, "Stratton–Chu vectorial diffraction of electromagnetic fields by apertures with application to small-Fresnel-number systems," J. Opt. Soc. Am. A **11,** 623–629 (1994).
8. A. Wang and A. Prata, Jr., "Lenslet analysis by rigorous vector diffraction theory," J. Opt. Soc. Am. A **12,** 1161–1169 (1995).
9. B. Richards and E. Wolf, "Electromagnetic diffraction in optical systems II. Structure of the image field in an aplanatic system," Proc. R. Soc. A **253,** 358–379 (1959).
10. M. Gu, *Advanced Optical Imaging Theory*, Vol. 75 of Springer Series in Optical Sciences (Springer-Verlag, Berlin, 2000).
11. J. W. M. Chon, X. Gan, and M. Gu, "Splitting of the focal spot of a high numerical-aperture objective in free space," Appl. Phys. Lett. **81,** 1576–1578 (2002).
12. M. Lax, "From Maxwell to paraxial wave optics," Phys. Rev. A **11,** 1365–1370 (1975).
13. Q. Cao and X. Deng, "Correction to the paraxial approximation of an arbitrary free-propagation beam," J. Opt. Soc. Am. A **15,** 1144–1148 (1998).
14. Q. Cao, "Correction to the paraxial approximation solutions in transversely nonuniform refractive-index media," J. Opt. Soc. Am. A **16,** 2494–2499 (1999).
15. A. I. Carswell, "Measurements of the longitudinal component of the electromagnetic field at the focus of a coherent beam," Phys. Rev. Lett. **15,** 647–649 (1965).
16. M. Born and E. Wolf, *Principles of Optics*, 7th ed. (Cambridge University, Cambridge, England, 1999).
17. J. E. Harvey, "Fourier treatment of near-field scalar diffraction theory," Am. J. Phys. **47,** 974–980 (1979).
18. W. H. Southwell, "Validity of the Fresnel approximation in the near field," J. Opt. Soc. Am. **71,** 7–14 (1981).
19. C. J. R. Sheppard and M. Hrynevych, "Diffraction by a circular aperture: a generalization of Fresnel diffraction theory," J. Opt. Soc. Am. A **9,** 274–281 (1992).
20. Y. Fainman and J. Shamir, "Polarization of nonplanar wave fronts," Appl. Opt. **23,** 3188–3195 (1984).